Coastal Engineering, 11 (1987) 329–351
Elsevier Science Publishers B.V., Amsterdam — Printed in The Netherlands

An Efficient Finite-Difference Approach to the Mild-Slope Equation

P.A. MADSEN and J. LARSEN

Danish Hydraulic Institute, Agern Allé 5, DK-2970 Horsholm, Denmark

(Received December 1, 1986; revised and accepted June 1, 1987)

ABSTRACT

Madsen, P.A. and Larsen, J., 1987. An efficient finite-difference approach to the mild-slope equation. *Coastal Eng.*, 11: 329–351.

A system of differential equations, the stationary part of which can be reduced to the elliptic mild-slope equation, is derived. The transient terms make the system of equations hyperbolic and similar to the system of equations governing nearly horizontal flow. The highly efficient ADI algorithm for the latter is used iteratively to find the stationary solution. By extracting the time-harmonic part and using a varying time step in the iterations the computational time is reduced greatly as compared with previous techniques.

INTRODUCTION

For a number of years mathematical short-wave models have been applied in engineering practice to assess the wave conditions in existing or proposed new harbours.

One of the most general approaches so far is based on the time-dependent, vertically integrated Boussinesq equations of conservation of mass and momentum (Abbott et al., 1981). This type of model system has been shown to be applicable to the analysis and solution of a number of practical engineering problems. The transformation of directional irregular nonlinear wave trains can be simulated in this type of model due to the inclusion of frequency and amplitude dispersion.

An alternative approach is based on the mild-slope equation as formulated by Berkhoff (1972). Models based on this equation can determine the motion of linear monochromatic waves in areas of moderate bottom slope. However, Booij (1983) has shown that acceptable results can be achieved even though the bottom slope is not moderate.

The approach based on the mild-slope equation supplements the more comprehensive approach based on the Boussinesq equations. For some applica-

0378-3839/87/$03.50

tions the latter is preferable: for instance for determining the short-wave disturbance in harbours where it is essential to simulate nonlinear irregular wave trains. However, for other applications such as harbour resonance studies or wave-induced currents in the surf zone, the mild-slope equation turns out to be preferable because of the reduction in the computational effort involved. One should bear in mind that the mild-slope equation deals with monochromatic waves only, so it becomes essential to have a very fast and efficient way of solving this equation.

The elliptic mild-slope equation is most commonly solved by finite-element techniques (Berkhoff, 1972; Chen and Mei, 1974; Behrendt and Jonsson, 1984). However, this method rapidly becomes expensive and eventually impossible for increasing model sizes.

The object of this paper is to present an approach by which large model areas can be handled with a relatively small amount of computational effort. By recasting the mild-slope equation as a system of first-order differential equations, which are similar to the system of equations governing nearly horizontal flow in shallow water, the highly efficient algorithms developed for the solution of the latter can be applied. The first stages of the model development were presented by Warren et al. (1985). A similar approach was presented by Copeland (1985) who solved the resulting system of hyperbolic equations using an explicit finite-difference scheme. In the present approach we have speeded up the algorithm by extracting the harmonic time variation from the differential equations and by solving the resulting complex equations by an implicit scheme using a time-varying time step.

FORMULATION OF THE EQUATIONS

The mild-slope equation, valid for steady-state solutions only, can be expressed by:

$$\nabla(CC_g \nabla\zeta) - \frac{C_g}{C}\frac{\partial^2\zeta}{\partial t^2} = 0 \tag{1}$$

where ζ is the surface elevation, C is the phase velocity, C_g is the group velocity, ∇ is the horizontal gradient operator.
The phase velocity and the group velocity are related to the local still water depth $h = h(x,y)$ through the equations:

$$C^2 = (g/k)\tanh(kh)$$

and

$$C_g = 1/2[1 + 2kh/\sinh(2kh)]C$$

where k is the local wave number.

As shown by Copeland (1985), eqn. (1) can be rewritten as a system of first-order equations by introducing the pseudo fluxes P^* and Q^*:

$$\frac{\partial P^*}{\partial t}+C\,C_g\frac{\partial \zeta}{\partial x}=0$$

$$\frac{\partial Q^*}{\partial t}+C\,C_g\frac{\partial \zeta}{\partial y}=0 \qquad (2)$$

$$\frac{C_g}{C}\frac{\partial \zeta}{\partial t}+\frac{\partial P^*}{\partial x}+\frac{\partial Q^*}{\partial y}=0$$

This system of equations is clearly similar to the mass and momentum equations governing nearly horizontal flow in shallow water.

A time-stepping integration of eqn. (2) is actually an iteration towards the steady-state solution. Hence, although the numerical solution to eqn. (2) will have a transient nature, only the final (steady-state) solution is a solution to the original elliptic mild-slope equation.

Copeland (1985) solved eqn. (2) by using an explicit finite-difference scheme with a time step restricted by a Courant number of 1.

In the present approach we speed up the solution considerably by reformulating the equations. First of all, the harmonic time variation is extracted from the equations by inserting:

$$\begin{aligned}\zeta &= S(x,y,t)\,e^{i\omega t}\\ P^* &= P(x,y,t)\,e^{i\omega t}\\ Q^* &= Q(x,y,t)\,e^{i\omega t}\end{aligned} \qquad (3)$$

where ω is the cyclic wave frequency and S, P and Q are complex functions of x and y.

As indicated S, P and Q are also slowly varying with t due to the iterative procedure in determining the steady-state solution.

By inserting eqn. (3) into eqn. (2) and by generalizing the equations to include internal generation of waves (source terms), we obtain the following set of equations:

$$\begin{aligned}\lambda_1\frac{\partial S}{\partial t}+\lambda_2 S+\frac{\partial P}{\partial x}+\frac{\partial Q}{\partial y} &= SS\\ \lambda_3\frac{\partial P}{\partial t}+\lambda_4 P+C_g^2\frac{\partial S}{\partial x} &= 0\\ \lambda_3\frac{\partial Q}{\partial t}+\lambda_4 Q+C_g^2\frac{\partial S}{\partial y} &= 0\end{aligned} \qquad (4)$$

where

$$\lambda_1 \equiv \frac{C_g}{C} \quad , \quad \lambda_3 = \frac{C_g}{C}$$
$$\lambda_2 \equiv \frac{C_g}{C} i\omega \quad , \quad \lambda_4 = \frac{C_g}{C} i\omega \qquad (5)$$

and where SS is the source term which generates the incoming wave.

INTERNAL GENERATION OF WAVES

The time-harmonic waves are generated internally inside the model boundaries using a source term in the mass equation. This technique is described by Larsen and Dancy (1983).

Along each generation line a certain amount of water is added. The added volume is determined as:

$$q_{wave}\, \Delta s\, \Delta t \qquad \left(\frac{m^2}{s}\, m\, s\right)$$

where q_{wave} is the "pseudo flux" in a progressive wave, Δs is the width of the wave front inside a grid mesh, Δt is the time step.

The pseudo flux in a progressive wave can be found by assuming a constant form solution to the mild-slope equation (2). On a horizontal bottom this leads to:

$$q_{wave} = C_g\, \zeta(t)$$

where $\zeta(t)$ is the surface elevation of the incoming wave and C_g is the group velocity.

The source term in eqn. (4) can now be determined as the added volume of water divided by the area of the grid mesh and Δt. Hence, considering a time-harmonic input wave with an amplitude of unity, we get:

$$SS = C_g \left(\frac{\Delta s}{\Delta x \Delta y}\right) \qquad (6)$$

The added amount of water will propagate in two opposite directions hence only half of the specified wave energy will enter the area of interest (Fig. 1). Therefore, two parallel generation lines will be specified in order to obtain an incoming wave amplitude of unity.

As shown by Larsen and Dancy (1983), reflected waves are allowed to cross the generation lines without any distortion or reflection.

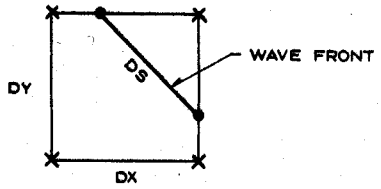

Fig. 1. Definition sketch internal generation of waves.

PARTIAL REFLECTION FROM BREAKWATERS

Having rewritten the mild-slope equation as a set of mass and momentum-type equations it is quite easy to transfer some of the techniques developed for the equations governing nearly horizontal flow in shallow water to the problem.

For instance Madsen and Warren (1983) have shown that the partial reflection from piers and breakwaters can be simulated by generalizing the mass and momentum equations to describe the flow inside a vertical porous rubble mound. The equations include the porosity of the rubble mound and a nonlinear friction term describing the laminar and turbulent energy loss inside the porous structure. By varying the value of the porosity from the value of 1 in open water to a value between 1 and 0 inside the porous structure, partial reflection and transmission can be simulated. Furthermore, Madsen (1983) has shown how a general nonlinear friction term can be linearized by applying the Lorentz principle of equivalent work. The resulting linear friction factor f_n describing the laminar and turbulent energy loss depends on the following quantities: the porosity n, the width of the absorber, the grain size, the water depth, the wave period and the incoming wave amplitude.

By comparing the mild-slope equation in the form of eqn. (2) or eqn. (4) with the equations solved by Madsen (1983), it is readily seen that the effect of the rubble mound can be included by modifying the coefficients in eqn. (5) to:

$$\lambda_1 = n\frac{C_g}{C} \quad , \quad \lambda_3 = \frac{1}{n}\frac{C_g}{C}$$

$$\lambda_2 = n\frac{C_g}{C}\,i\omega \quad , \quad \lambda_4 = \frac{C_g}{C}\frac{\omega}{n}\,(i+f_n)$$

where f_n is the linear friction factor due to the energy loss inside the porous structure and n is the porosity.

ABSORPTION WITH SPONGE LAYER

Almost perfect absorption of waves can be obtained by using the sponge layer technique described by Larsen and Dancy (1983). This technique is based

on artificial damping which is introduced in the governing equations by applying a linear friction factor, f_s, in a few grid lines in the vicinity of the closed boundaries. It appears that the most efficient absorption can be obtained if the damping intensity is gradually increased from the water area to the closed boundary. The sponge layers have very broad-banded damping characteristics and using only 5 grid lines of damping leads to reflection coefficients of less than 7% even with only 5% of the wave length in the sponge layer. By comparing the mild-slope equation in the form of eqns. (2) or (4) with the equations considered by Larsen and Dancy (1983) it is readily seen that the effect of the sponge layer can be included by modifying the coefficients in eqn. (5) to:

$$\lambda_2 = \frac{C_g}{C} i\omega + f_s$$

$$\lambda_4 = \frac{C_g}{C} i\omega + f_s$$

where f_s is the friction factor due to the sponge layer absorption (see Larsen and Dancy, 1983).

THE NUMERICAL SCHEME

The differential equations (4) are equivalent to the system of equations governing nearly horizontal flow in shallow water. Hence the efficient algorithms developed for solving these equations can also be applied here.

An implicit finite-difference scheme is applied with the complex variables S, P and Q defined on a space-staggered rectangular grid. The normal ADI (alternating direction) algorithm is invoked and the equations are solved by means of the Double Sweep algorithm (a special form of Gauss elimination).

The following finite-difference formulation is applied:

X-sweep:

$$\lambda_1 \frac{2}{\Delta t}(S_{j,k}^{n+\frac{1}{2}} - S_{j,k}^{n}) + \frac{\lambda_2}{2}[(2-\delta)S_{j,k}^{n+\frac{1}{2}} + \delta S_{j,k}^{n}]$$

$$+\frac{1}{2\Delta x}[(2-\delta)(P_{j,k}^{n+1} - P_{j-1,k}^{n+1}) + \delta(P_{j,k}^{n} - P_{j-1,k}^{n})]$$

$$+\frac{1}{2\Delta y}[(2-\delta)(Q_{j,k}^{n+\frac{1}{2}} - Q_{j,k-1}^{n+\frac{1}{2}}) + \delta(Q_{j,k}^{n-\frac{1}{2}} - Q_{j,k-1}^{n-\frac{1}{2}})] = SS_{j,k}^{n+\frac{1}{2}} \qquad (7a)$$

$$\frac{\lambda_3}{\Delta t}(P_{j,k}^{n+1}-P_{j,k}^{n})+\frac{\lambda_4}{2}[(2-\delta)P_{j,k}^{n+1}+\delta P_{j,k}^{n}]+C_g^2\frac{1}{\Delta x}(S_{j+1,k}^{n+\frac{1}{2}}-S_{j,k}^{n+\frac{1}{2}})=0 \qquad (7b)$$

Y-sweep

$$\lambda_1\frac{2}{\Delta t}(S_{j,k}^{n+1}-S_{j,k}^{n+\frac{1}{2}})+\frac{\lambda_2}{2}[(2-\delta)S_{j,k}^{n+1}+\delta S_{j,k}^{n+\frac{1}{2}}]$$

$$+\frac{1}{2\Delta x}[(2-\delta)(P_{j,k}^{n+1}-P_{j-1,k}^{n+1})+\delta(P_{j,k}^{n}-P_{j-1,k}^{n})]$$

$$+\frac{1}{2\Delta y}[(2-\delta)(Q_{j,k}^{n+3/2}-Q_{j,k-1}^{n+3/2})+\delta(Q_{j,k}^{n+\frac{1}{2}}-Q_{j,k-1}^{n+\frac{1}{2}})]=SS_{j,k}^{n+1} \qquad (8a)$$

$$\frac{\lambda_3}{\Delta t}(Q_{j,k}^{n+3/2}-Q_{j,k}^{n+\frac{1}{2}})+\frac{\lambda_4}{2}[(2-\delta)Q_{j,k}^{n+3/2}+\delta\, Q_{j,k}^{n+\frac{1}{2}}]$$

$$+C_g^2\frac{1}{\Delta y}(S_{j,k+1}^{n+1}-S_{j,k}^{n+1})=0 \qquad (8b)$$

where the subscript j is the increment in the x-direction and k is the increment in the y-direction. The superscript n is the increment in time.
During the x-sweep P^{n+1} and $S^{n+1/2}$ will be determined while the following y-sweep will determine $Q^{n+3/2}$ and S^{n+1}.

Notice that the parameter δ has the following role:

$$\delta=\begin{cases}2\Rightarrow\text{backward centering}\\ 1\Rightarrow\text{mid-centering}\\ 0\Rightarrow\text{forward centering}\\ -1\Rightarrow\text{extrapolation}\end{cases}$$

Accurate dynamic solutions are normally obtained by using $\delta=1$ while it appears to be an advantage to use $0\leqslant\delta<1$ for steady-state problems.

After a certain number of iterations (i.e. time steps), the steady-state solution $S^{\infty}(x,y)$ is obtained and the disturbance coefficients (relative wave heights) can be determined as the moduli of S^{∞}.

In the following we will discuss how to minimize the number of time steps or iterations needed to achieve the steady-state solution.

USING A FIXED TIME STEP

Usually the time step and the grid size will be restricted by the resolution of the wave period, T, and the wave length, L. If we define this resolution by:

$$N^t \equiv \frac{T}{\Delta t} \quad \text{and} \quad N^x \equiv \frac{L}{\Delta x} \tag{9a}$$

we can express the Courant number by:

$$CR = \frac{N^x}{N^t} \tag{9b}$$

Solving the hyperbolic equations (2) directly (as done by Copeland, 1985) requires N^x and N^t of the order 10 and a Courant number of the order 1. Copeland found that accurate results could only be obtained with $N^x > 20$ and $CR < 1$.

Now the significant advantage in extracting the harmonic time variation from the differential equations before a finite-difference scheme is applied is that one does not need to resolve the wave period any longer. Only the transient time variation is left in eqns. (4) and it should be expected that a much larger Courant number can be used in the iteration process.

The first trial runs with the model partly confirmed this expectation and a series of one-dimensional channel tests were made with different values of the Courant number CR and of the centering factor δ (see eqns. 7 and 8). The solutions appeared to be quite sensitive to the value of δ: It was found that using $\delta = 1$ (i.e. mid-centering) made the computed solution oscillate around the exact solution and for $CR > 100$ the x- and y-sweep solutions began to diverge even though this was a purely one-dimensional problem.

However, using $\delta = 0$ (i.e. forward centering) made the numerical solution converge without any oscillations at all and furthermore there seemed to be no limitation on the Courant number. We finally used a Courant number of infinity corresponding to neglecting the time derivatives in eqn. (4) and determined the exact solution of a standing wave pattern in one single sweep.

This result was of course very promising but turning to two-dimensional problems we quickly ran into trouble. As already found from the one-dimensional tests a smooth convergence could only be achieved with δ close to zero. However, the two-dimensional tests showed that an increase in the Courant number would require an increase in δ as well in order to avoid instabilities. This was confirmed by a Fourier stability analysis made for CR equal to infinity. This analysis showed that in the one-dimensional case δ can be chosen freely while the two-dimensional case requires $\delta \geqslant 1$ in order to avoid instabilities. On the other hand, the analysis also showed that although the numerical scheme is stable for $CR = \infty$ and $\delta = 1$ the solutions obtained after the x-sweep and after the y-sweep are completely unconnected. Hence one can achieve an extremely fast and stable solution which has nothing to do with the exact solution.

Naturally, trial runs were made with moderate values of both parameters such as $CR = 10$ and $0 < \delta < 1$ but although the numerical scheme appeared to

be stable for quite some time it eventually broke down as soon as the deviations from the exact solution became small. It was finally concluded that if we use a fixed time step, the present scheme requires forward centering (i.e. $\delta = 0$) and a Courant number of the order 1 to give a smooth and stable convergence.

This conclusion was rather disappointing because a much higher speed of convergence was expected and therefore we started to consider using a time-varying time step with the forward centered scheme (i.e. $\delta = 0$).

USING A TIME-VARYING TIME STEP

The following computerized strategy for completely automatic change of the time step has been adopted:
Every time step comprises two standard double sweeps with the present value of Δt plus one extra book-keeping double sweep with the double value of Δt. After each time step the test parameter TP is determined by:

$$TP \equiv \frac{\|S^n - S^n_*\|}{\|S^n - S^{n-1}\|}$$

where S^{n-1} is the value of the surface elevations obtained from the previous time step, S^n is the value obtained from the new first two double sweeps (using Δt) and S^n_* is the value obtained from the book-keeping double sweep (using $2\Delta t$).
The actual computation of the norm is done in the following way:

$$\|S^n - S^{n-1}\| = \sqrt{\sum_i \sum_j \mathrm{ABS}(S^n_{ij} - S^{n-1}_{ij})^2}$$

Now the strategy adopted for the automatic change of Δt is the following. When TP falls in the intervals: [0,0.05], [0.05,0.10], [0.10,0.15], [0.15,0.30], [0.30,0.40], [0.40,0.60], one accepts the present computation and changes Δt by a factor 4, 2, 1.5, 1, 1/2, 1/4 respectively, for the next time step. However, when TP falls in the interval [0.6,∞] one rejects the present computation and starts the step again with Δt changed by a factor 1/16.

This strategy for automatic change of the time step is almost identical to the one suggested by Doss and Miller (1979). Clearly, the determination of TP is an expensive one but this parameter is actually a very good indicator of growing instabilities.

This can be illustrated by the following diffraction test (Fig. 2): The model area comprises 100×100 grid points corresponding to a N^x of approximately 10. All four boundaries are closed and the waves are generated internally along grid lines 6 and 7 at the southern boundary. Sponge layer absorption is applied along the northern and eastern boundaries in order to minimize reflections. Full reflection will occur along the western boundary and along the southern

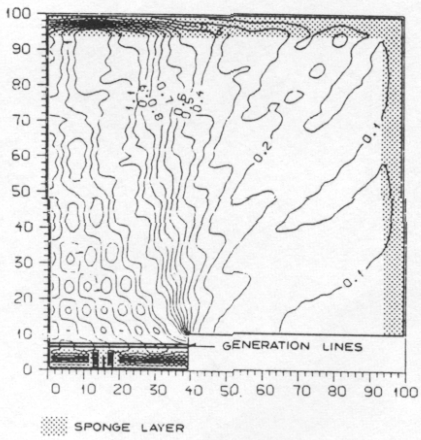

Fig. 2. Diffraction test. Grid size = 9.35 m ($N^x = 10$), water depth = 10.2 m, wave period = 10 s.

breakwater. The simulation has been continued for 100 iterations each comprising 2 double sweeps. A fixed time step corresponding to a Courant number of 1 has been used. Figure 2 shows the resulting isolines of the relative wave heights.

Notice that due to the diffraction from the edge of the breakwater, wave disturbance propagates towards the western boundary from which it is fully reflected. This is the reason for the undulations of the isolines on the leeward side of the breakwater.

The next step has been to repeat this test with a fixed time step corresponding to a Courant number of 2. As a measure of the quality of the solution during the iteration, the parameter:

$$RDN \equiv \frac{\|S^n - S^{n-1}\|}{\|S^n\|}$$

has been computed together with TP for every second double sweep (Fig. 3). After 20 iterations the steady-state solution has almost been achieved and the value of RDN has dropped to only 0.01.

However, continuing the simulation makes the RDN grow again between iteration number 25 and 60 and the actual solution goes completely wrong. This is the type of instability discussed in the previous section. However, it is seen that the parameter TP quickly indicates the coming instability by a rapid increase after approximately 20 iterations.

The way of avoiding the instability is to switch on the automatic determination of the time step. This has been done in Fig. 4 and first of all it is noticed that the value of RDN remains very low during the full computation. There are 2 spikes in the TP variation (after 20 and 90 iterations). These indicate a coming instability which is then avoided by the automatic switch to a lower

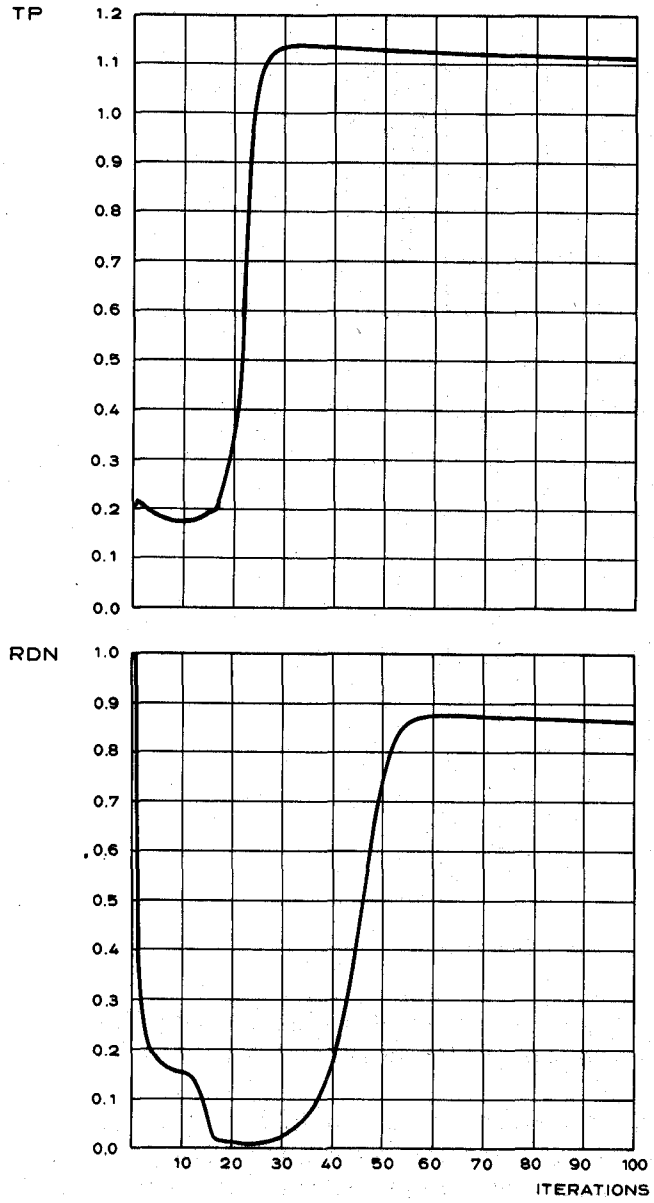

Fig. 3. Diffraction test. Fixed time step, Courant number = 2.

time step. After 21 iterations the *RDN* has decreased to 0.005 and after 100 iterations the value has dropped to only 0.0003.

Naturally, there is no need to continue the iterations until the *RDN* value drops to almost zero, and choosing a reasonable stop criterion is very important

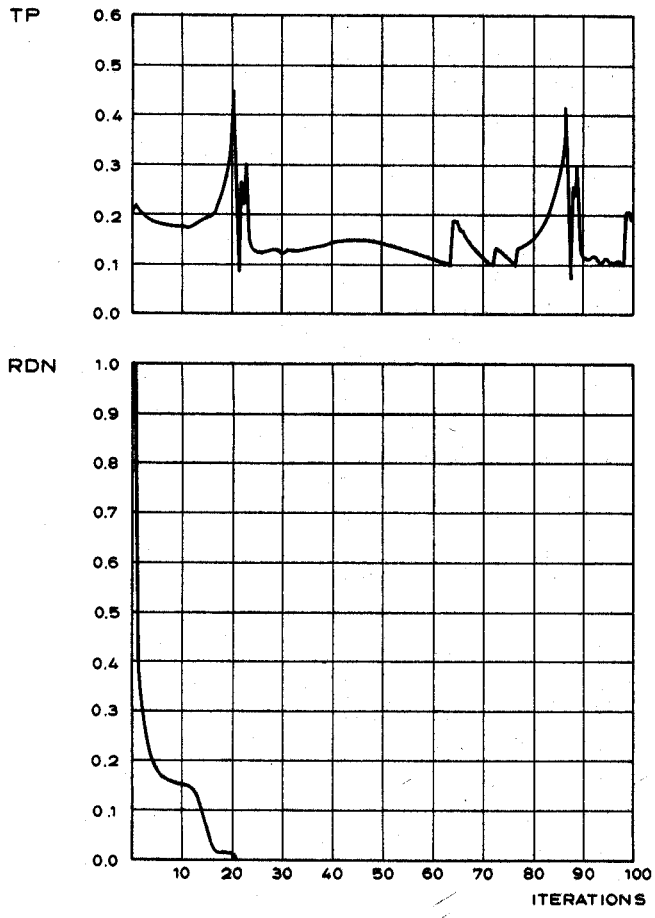

Fig. 4. Diffraction test. Automatic change of time step.

in order to achieve an efficient and economic algorithm. Actually, Doss and Miller (1979) did not suggest any criteria for the general case where the exact solution is not known.

At first glance it appears that a certain low value of *RDN* could be used as a stop criterion. However, it turns out that this parameter is not adequate unless we use a fixed time step because the value of *RDN* will depend on the local size of the time step. Hence a stop criterion based on *RDN* would typically be activated in case of a growing instability because the automatic strategy would respond with a considerable decrease of the time step which could lead to a very low value of *RDN*.

Instead it appears that a stop criterion should be based on the following convergence parameter:

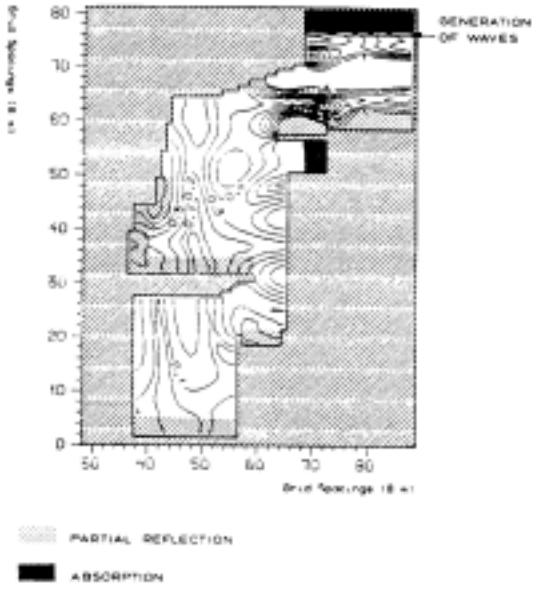

Fig. 5. Amplification factors. Model data: grid size = 8 m; initial time step = 0.8 s; water depth = 8 m; wave period = 18 s. Result after 28 iterations.

$$CP = \frac{\|S^n - S^{n-1}\|}{\|S^n\|}\sqrt{\alpha}$$

where α is the ratio between the initial time step and the local time step. The initial time step is chosen corresponding to a Courant number of 1. The iteration for the steady-state solution is stopped when CP drops below 0.005.

APPLICATIONS OF THE MODEL

In order to investigate a possible resonance occurring in the inner basin of the harbour shown in Fig. 5, simulations have been made with a range of wave periods. As an example, Fig. 5 shows the computed amplification factors (relative wave heights) for a wave period of 18 s. The steady-state solution has been obtained after 28 iterations with a time varying time step. The waves are generated internally in the northern part of the model. Partial reflection is taken into account by applying porosity layers along a number of the breakwaters. It should be mentioned that the result shown in Fig. 5 agrees perfectly with relative RMS-values of results computed by a model based on the time-dependent Boussinesq equations (using small wave heights and regular wave input).

It is a well known problem to resolve correctly a breakwater at an angle to the rectangular grid. In this case the smooth fully or partially reflecting front face of the breakwater is replaced by a number of steps. The effect of these steps depends strongly on the number of grid points per wave length. If this

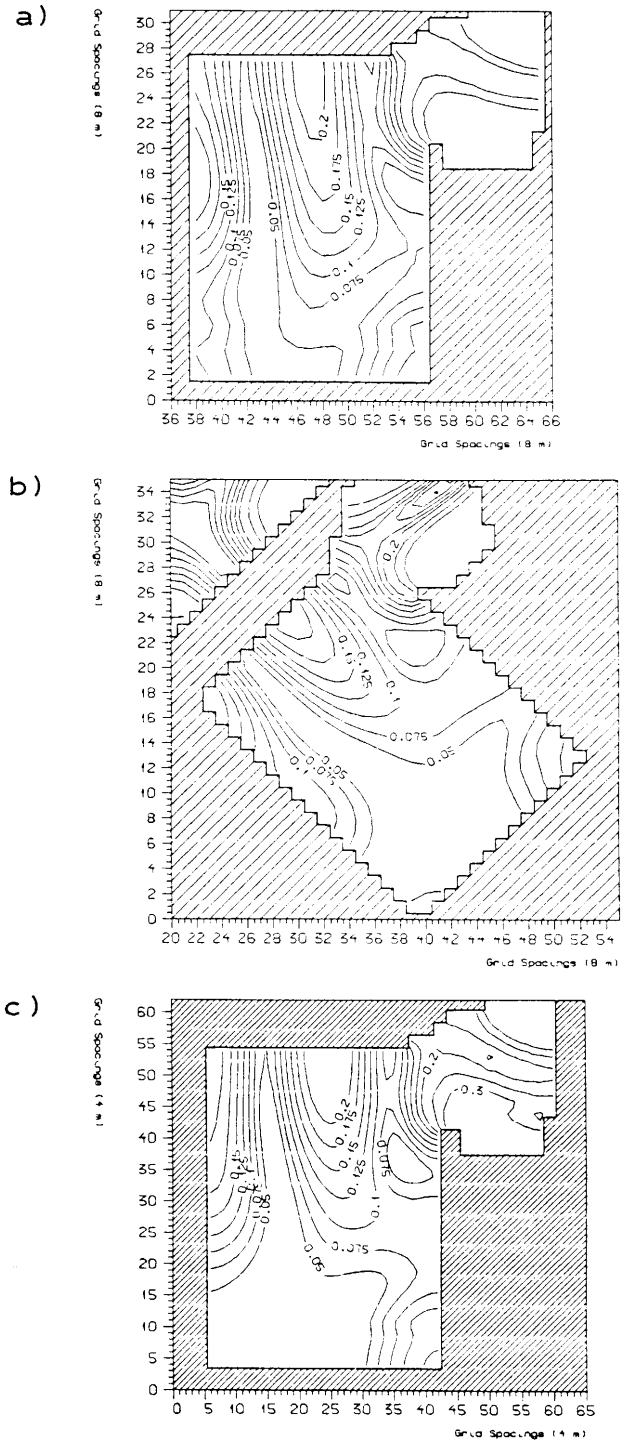

Fig. 6. Amplification factors (inner basin). Wave period = 18 s. (a) Grid size = 8 m. (b) Grid size = 8 m (topography turned 45°). (c) Grid size = 4 m.

TABLE 1

Diffraction and reflection test; model data: grid size - 8 m; initial time step - 0.8 s; water depth - 8 m; number of grid points - 89×81

T (s)	N^x	α_{min}	min(N^t)	No. of iterations	CPU (s)
9[a]	9.3	—	—	>200	—
10	10.5	0.38	4.7	83	139
11	11.6	0.38	5.2	89	148
12	12.8	0.28	4.2	97	161
13	13.9	0.28	4.6	83	138
14	15.1	0.28	4.9	34	59
15	16.2	0.28	5.3	34	59
18	19.6	0.21	4.7	28	49
24	26	0.21	6.3	26	46

[a]No convergence.

number is too low (say less than 10 points) the wave disturbance will be exaggerated close to the breakwater. In Fig. 6a and 6b we have shown what happens if the harbour (from Fig. 5) is turned 45 degrees. The grid size is 8 m corresponding to 20 points per wave length. The computed disturbance factors show a remarkable agreement.

The effect of refining the grid size is also illustrated in Fig. 6c. Clearly it makes almost no difference whether the grid size is 8 or 4 m corresponding to 20 and 40 grid points per wave length respectively. However, as we shall see later, it does make a difference going from 20 to 10 grid points.

Tables 1 and 2 summarize the efficiency of the automatic strategy for choosing optimal time steps in the iteration for steady-state solutions to the problem shown in Fig. 5.

In Table 1 the grid size is 8 m and the wave period has been varied from 9 to 24 s. First of all we notice that the steady-state solution is obtained much faster for the long periods than for the short periods. For T=24 s the solution is obtained after only 26 iterations and a CPU time of 46 s on an IBM 3033. If we had used a fixed time step corresponding to a Courant number of 1 it would have required approximately 150 iterations and a CPU time of 120 s. For wave periods shorter than 14 s the efficiency of the scheme drops considerably and for wave periods shorter than 10 s a steady-state solution is not obtained at all. Hence it appears that the efficiency of the scheme is very sensitive to the number of grid points per wave length.

This observation is confirmed by Table 2 where the grid size is only 4 m and the wave periods have been varied from 24 to 6 s. For T=24 s the solution is obtained after 27 iterations and a CPU time of 148 s. Hence a refinement of the grid size has not increased the CPU time with the normal factor 8 but only

TABLE 2

Diffraction and reflection test; model data: grid size - 4 m; initial time step - 0.4 s; water depth - 8 m; number of grid points - 108×162.

T (s)	N^x	α_{min}	min(N^t)	No. of iterations	CPU (s)
6[a]	11.3	—	—	>300	—
7	13.8	0.21	3.7	137	727
8	16.2	0.21	4.2	126	671
9	18.6	0.21	4.7	41	223
10	21.0	0.21	5.3	41	222
11	23.3	0.16	4.4	40	217
12	25.6	0.16	4.8	38	206
15	32.4	0.16	6.0	33	180
18	39.2	0.12	5.4	30	164
24	52	0.12	7.2	27	148

[a]No convergence.

with a factor 3.2! If a fixed time step had been applied it would have required a CPU time of approximately 960 s. According to Table 2 the efficiency of the scheme drops considerably for wave periods shorter than 9 s corresponding to 19 grid points per wave length. For wave periods shorter than 6–7 s (corresponding to approximately 12 points per wave length) steady-state solutions cannot be obtained.

Comparing Tables 1 and 2 it appears that in order to achieve an efficient convergence towards the steady-state solution we should allow for at least 15–17 grid points per wave length. Copeland (1985) found that in the case of strong reflections he had to use more than 21 grid points per wave length in order to achieve reliable results. This is due to the complicated standing wave patterns where the distance between nodal and anti-nodal points is only $L/4$. Hence, iterating on the wave envelope obviously requires at least 4 grid points between the maximum and the minimum level. In other types of problems where the reflections are weak 8–10 grid points are sufficient (see Fig. 2).

By comparing Tables 1 and 2 we notice that, although the grid size has been refined by a factor 2, the time step chosen by the automatic strategy leads to almost the same minimum values of N^t. This quantity is always found in the interval 3–8 which means that the automatic strategy chooses a larger Courant number for larger values of N^x.

On Fig. 7 the results from Tables 1 and 2 have been combined to give the variation of the maximum Courant number as a function of N^x. The results obtained with grid size 8 m and with 4 m are very similar when they are presented in terms of N^x instead of T.

On Fig. 8 the efficiency is shown as a function of N^x. This efficiency has

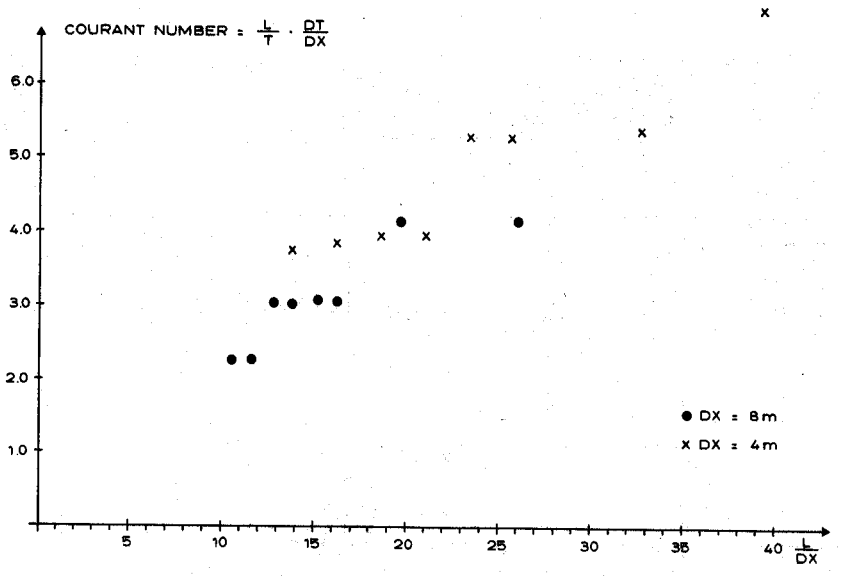

Fig. 7. The maximum Courant number chosen by the automatic strategy.

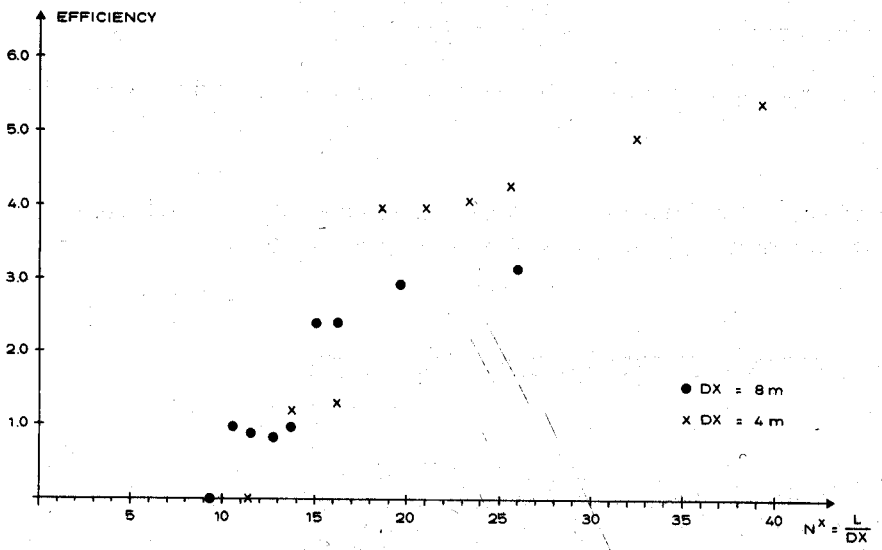

Fig. 8. Efficiency of the iteration scheme.

been defined as the distance between the entrance and the inner harbour (measured in number of grid points) divided by the number of iterations necessary to obtain a steady state solution. Using a fixed time step corresponding to a Courant number of 1 would lead to an efficiency of 1 in the case of weak reflections and approximately 0.5 in the case of strong reflections. Using the automatic strategy leads to an efficiency higher than 3 for N^x larger than 18.

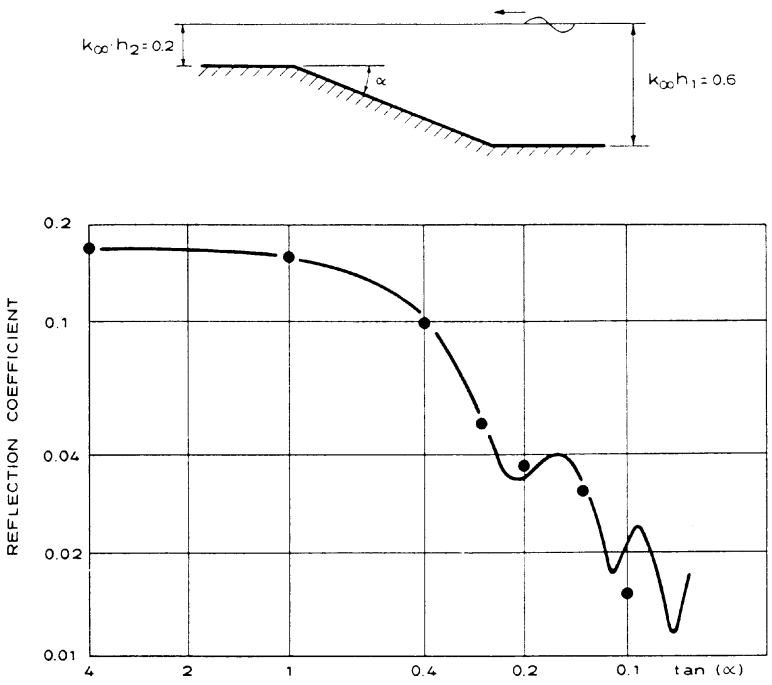

Fig. 9. Reflection from a sloping beach. ● = computed in this paper; — = mild-slope equation, Booij 1983.

In Fig. 9 the reflection from a sloping beach has been determined. The agreement with the results of Booij (1983) is seen to be excellent.

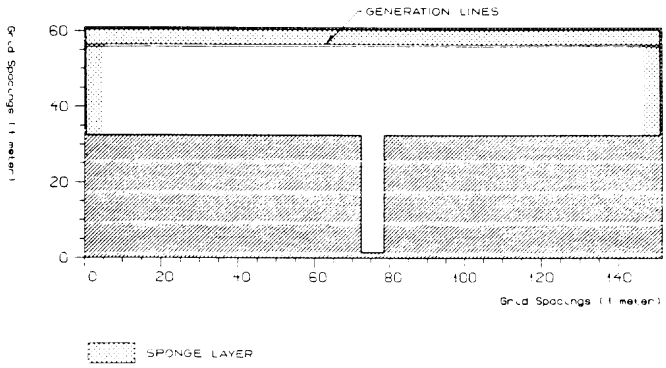

Fig. 10a. Model setup. Water depth = 25.73 m, width of basin = 6.0 m, length of basin = 31.0 m, grid size = 1.0 m.

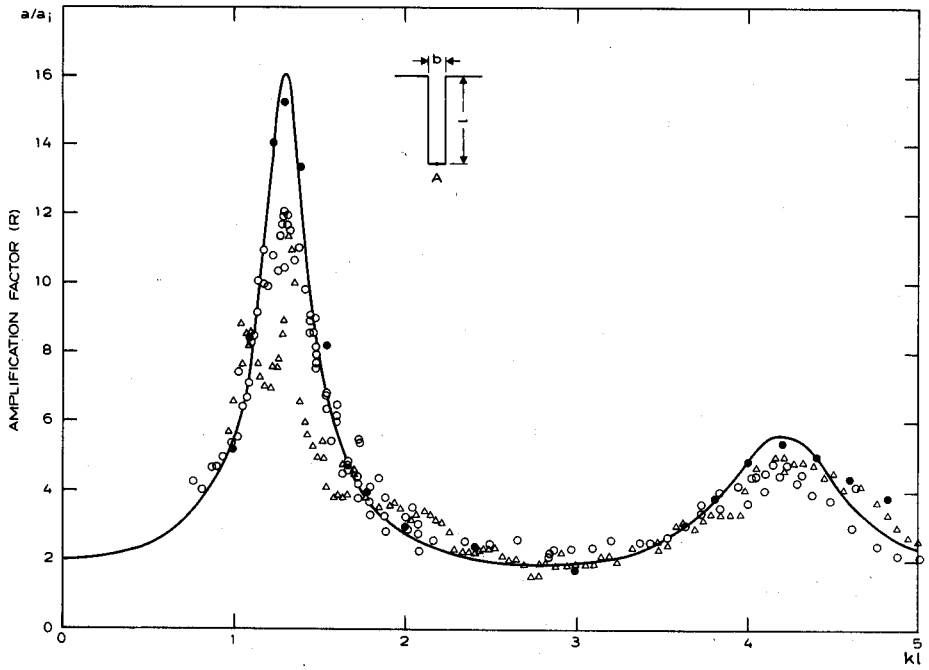

Fig. 10b. Amplification at the centre of the backwall of a fully open rectangular basin. ● = Computed by the present model. — = theoretical solution by Lee (1971). ○ = Experiment by Lee (1971). △ = Experiment by Ippen and Goda (1963).

In Fig. 10 harbour resonance in the classical fully open rectangular basin has been determined. Analytically, this is a relatively simple case to handle but numerically it is rather complicated to simulate for the following reasons: First of all the resonance depends entirely on the correct simulation of the partial reflection of waves at the entrance to the inner basin. This reflection will depend entirely on the width of the inner basin compared to the width of the outer basin which in principle should be infinity in this case. The model setup is shown in Fig. 10a: Absorbing sponge layers have been placed along all open boundaries and the incoming waves have been generated internally. The inner basin has been represented by 6×31 grid points and it has been necessary to make the outer basin 150 grid points wide (in order to represent the infinite open sea). Decreasing this width of the outer basin will decrease the peak of the amplification factor.

The computed amplification at the centre of the backwall of the inner basin has been compared to the theoretical solution by Lee (1971) and to the experimental results by Ippen and Goda (1963) and Lee (1971). The agreement is seen to be very good (Fig. 10b).

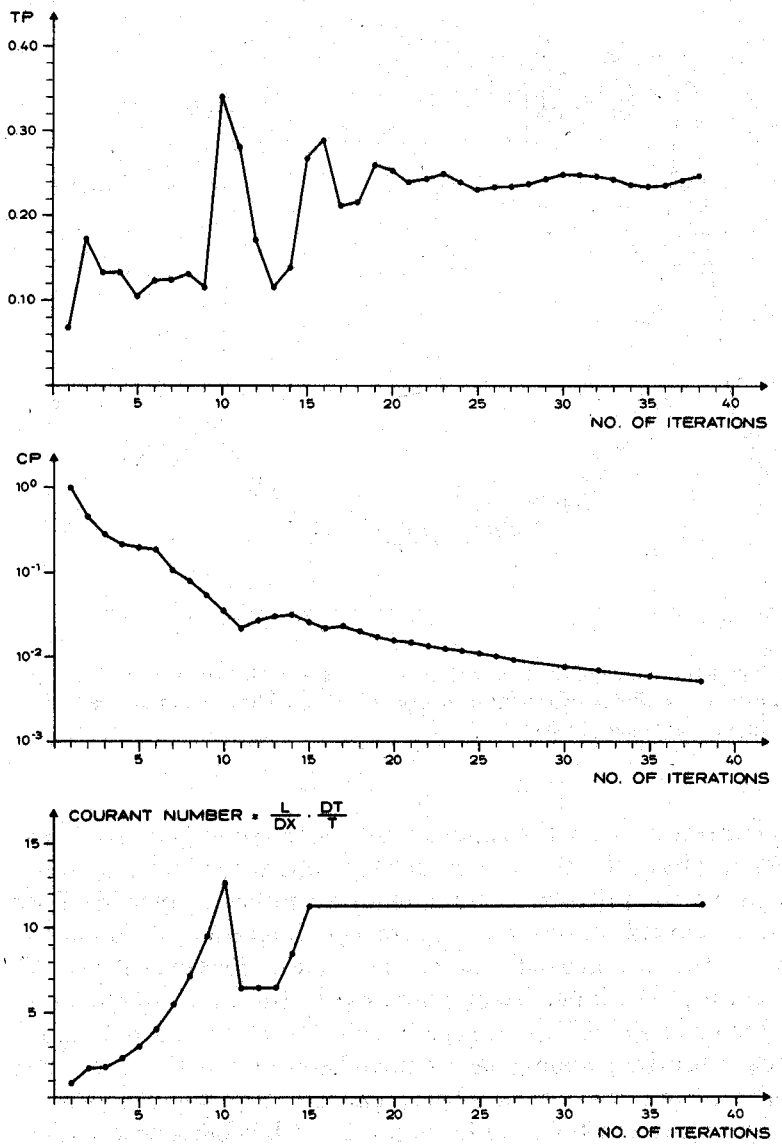

Fig. 10c. Time variation of *TP*, *CP* and the Courant number.

The wave number has been varied from 0.83 to 4.0 leading to 195 and 40 grid points per wave length, respectively. Steady-state solutions have been achieved after approximately 30 time steps using a maximum Courant number of 13.

For comparison it should be mentioned that using a model based on the time-dependent Boussinesq equations for this study would require more than 1500 time steps in order to obtain the steady-state solution.

In Fig. 10c a typical variation of *TP*, *CP* and of the Courant number is shown. Notice that the *CP* parameter is almost independent of the local value of the time step. Hence, this parameter is a reliable measure of the convergence of the solution.

Finally, Fig. 11 shows the development in time of the waves generated by a point source in a square basin with fully reflecting walls. The iteration is not

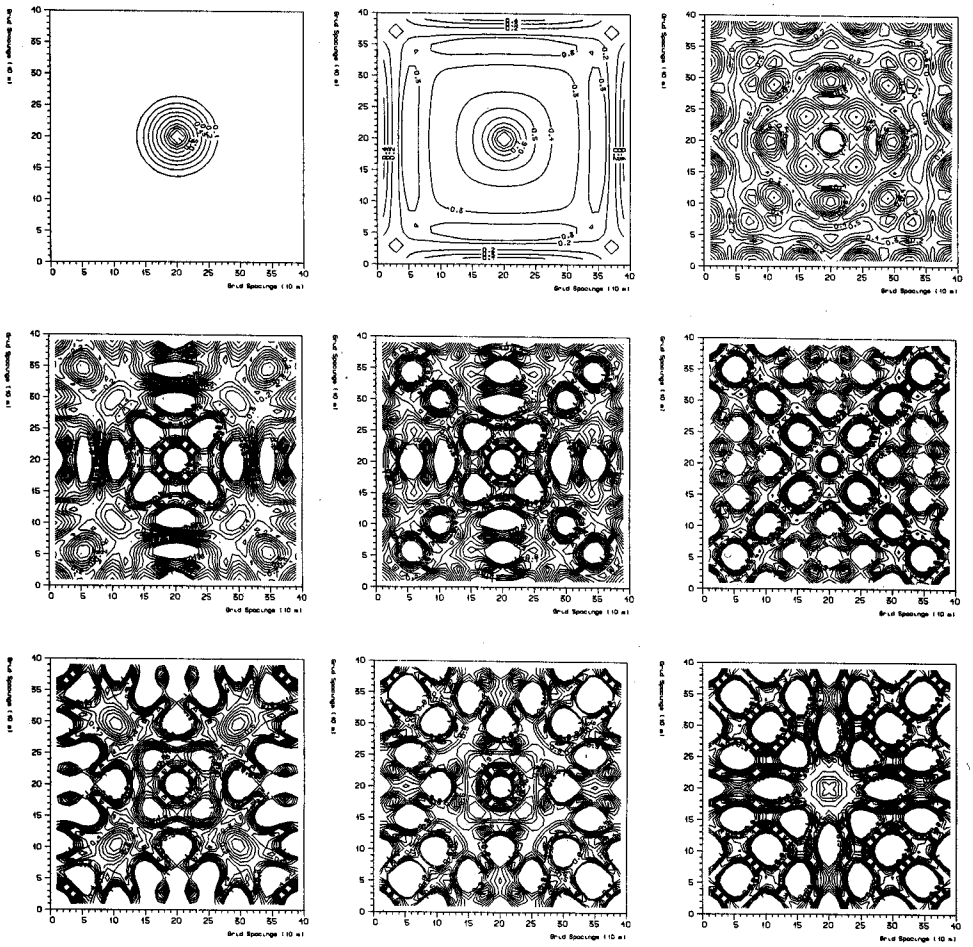

Fig. 11. Internal generation of waves in a single source point in a square fully reflecting basin. Isolines of amplification factors during different stages of the simulation.

convergent, since energy is constantly put into the basin and no energy is removed. The symmetry of the solution is maintained even at a late stage of the iteration thus demonstrating the robustness of the algorithm.

CONCLUSION

A finite-difference scheme based on the transient form of the mild-slope equation has been derived. A highly efficient ADI algorithm is used iteratively to find the stationary solution. The scheme depends on a centering parameter and the resolution in space and time. For the resolution of a standing wave pattern at least 16 grid points per wave length of the incident wave is needed. One-dimensional simulations show that forward centering enhances the convergence rate; but a fixed time step with a forward centered scheme leads to instabilities in the two-dimensional case. A strategy with a forward centered difference scheme and a time-varying time step leads to a stable convergent algorithm, which is faster than previous solution techniques.

ACKNOWLEDGEMENT

The work described in this paper has been supported by the Danish Technical Research Council and their help is gratefully acknowledged.

REFERENCES

Abbott, M.B., McCowan, A. and Warren, I.R., 1981. Numerical modelling of free-surface flows that are two-dimensional in plan. In: Transport Models for Inland and Coastal Water. Symposium on Predictive Ability, Academic Press.

Behrendt, L. and Jonsson, I.G., 1984. The physical basis of the mild-slope equation. Proc. 19th Coastal Eng. Conf., Houston 1984, ASCE.

Berkhoff, J.C.W., 1972. Computations of combined refraction-diffraction. Proc. 13th Coastal Eng. Conf., Chapter 24.

Booij, N., 1983. A note on the accuracy of the mild-slope equation. Coastal Eng., 6: 255–279.

Chen, H.S. and Mei, C.C., 1974. Oscillations and wave forces in an offshore harbour. Massachussetts Institute of Technology, Parsons Laboratory, Rep. No. 190.

Copeland, G.J.M., 1985. A practical alternative to the mild-slope wave equation. Coastal Eng., 9: 125–149.

Doss, S. and Miller, K., 1979. Dynamic ADI methods for elliptic equations. Siam J. Numer. Analysis, Vol. 16(5), Oct. 1979.

Ippen, A.T. and Goda, Y., 1963. Wave-induced oscillations in harbours: The solution for a rectangular harbour connected to the open-sea. Hydrodynamics Lab, M.I.T., T.R. No. 59.

Larsen, J. and Dancy, H., 1983. Open boundaries in short-wave simulations — A new approach. Coastal Eng., 7: 285–297.

Lee, Jiin-Jen, 1971. Wave-induced oscillations in harbours of arbitrary geometry. J. Fluid Mech., 45: 375–394.

Madsen, P.A. and Warren, I.R., 1983. Performance of a numerical short-wave model. Coastal Eng., 8: 73-93.

Madsen, P.A., 1983. Wave reflection from a vertical permeable wave absorber. Coastal Eng., 7: 381-396.

Warren, I.R., Larsen, J. and Madsen, P.A., 1985. Application of short wave numerical models to harbour design and future development of the model. Int. Conf. on Numerical and Hydraulic Modelling of Ports and Harbours, Birmingham, April 1985.